Motion of spiral tip driven by local forcing in excitable media*

Liu Gui-Quan(刘贵泉)[a)b)†] and Ying He-Ping(应和平)[a)‡]

[a)] *Zhejiang Institute of Modern Physics and Department of Physics, Zhejiang University, Hangzhou* 310027, *China*
[b)] *College of Science, China Jiliang University, Hangzhou* 310018, *China*

(Received 10 October 2013; revised manuscript received 25 November 2013; published online 25 March 2014)

We study the motion of a spiral wave controlled by a local periodic forcing imposed on a region around the spiral tip in an excitable medium. Three types of trajectories of spiral tip are observed: the epicycloid-like meandering, the resonant drift, and the hypocycloid-like meandering. The frequency of the spiral is sensitive to the local periodic forcing. The dependency of spiral frequency on the amplitude and size of local periodic forcing are presented. In addition, we show how the drift speed and direction are adjusted by the amplitude and phase of local periodic forcing, which is consistent with a theoretical analysis based on the weak deformation approximation.

Keywords: spiral wave, local forcing, resonant drift, weak deformation approximation

PACS: 05.45.–a, 05.45.Xt, 82.40.Ck, 82.20.–w **DOI:** 10.1088/1674-1056/23/5/050502

1. Introduction

A variety of spatiotemporal patterns can be triggered by finite perturbations in excitable media far from equilibrium, such as solitary waves, target waves, and spiral waves.[1] Among these patterns, the spiral wave is probably the most striking and frequently observed in various biological,[2,3] physical,[4] and chemical[5–7] systems. By changing the parameters of the system or injecting an external perturbation, the stable rotating spiral will become meandering or even breakup. As we know, the motion of a spiral tip can exhibit rich dynamic behaviors.[8–11] Since the spiral tip can be viewed as a wave source, it is very important to study the behavior of the core region of a spiral wave.

The control of a spiral wave has attracted considerable attention in the last decade. Many schemes of suppression, transition, and straight-line drifting of spiral waves have been studied. For example, spiral waves have been controlled by injecting periodic forcing to the system,[12–17] external illuminations,[6,18–20] electric fields,[21–24] feedback,[25–28] and coupling interaction.[29,30] In addition, the parameter perturbation method has usually been used to control spiral waves.[31–38] In Ref. [31], Zhang *et al.* investigated the drift of the spiral's tip under different light gradients. Their experiments showed that the gradient was a precise method to control spiral waves. Deng *et al*. have observed that there are three kinds of motions: stable rotation, rebound of spiral tip from the boundary, and breakup by introducing the gradient distribution of parameters.[32] Ma *et al.* proposed a method to suppress turbulence and remove the spiral wave by modulating the parameters with a weak pulse.[33] Wu *et al*. confirmed that the spiral tip's motion can be controlled by constructing the local gradient around the tip by artificial means.[34]

Although many methods to control spiral waves and turbulence have been put forward, investigation in this field is still open. Up to now, the current clinical method still uses a large amplitude shock for defibrillation, which may damage the heart and cause serious pain. From this point of view, a promising control scheme using a local forcing with a small amplitude, called antitachycardia pacing (ATP), has been developed for defibrillation in cardiac tissue.[39,40] Many reports have pointed out that a resonant drift of the spiral would occur when the frequency of the external forcing is close to that of the spiral wave without perturbation. However, this conclusion was based on the assumption that the natural frequency of the spiral wave was not influenced by the external forcing or the parametric modulation. In fact, the external forcing injected into the system and the parametric modulation will result in a change of the rotating spiral wave or induce the drift of the spiral tip.[41,42] It is pointed out that most of these studies on spiral drift are usually driven by a global periodically external field. However, there are few studies of spiral drift by a local small amplitude forcing.

Based on the advantage of the local small amplitude forcing, in this paper we perform a numerical simulation to understand how to better control the spiral drift, which is induced by the low-amplitude local periodic forcing (LPF) located around the spiral tip. The rest of this paper is organized as follows. The mathematical model is presented in Section 2. In Sec-

*Project supported by the National Natural Science Foundation of China (Grant No. 11274271) and the Scientific Research Foundation of Education Bureau of Zhejiang Province, China (Grant No. Y201224250).

†Corresponding author. E-mail: gqliu@zju.edu.cn

‡Corresponding author. E-mail: hpying@zju.edu.cn

© 2014 Chinese Physical Society and IOP Publishing Ltd

tion 3, the numerical estimations are investigated, beginning with the motion of spiral tip under local forcing with different frequencies. Then, the evidence necessary to choose an appropriate frequency is presented for the realizations of resonance drift of the spiral with different radius of local forcing. Lastly, we observe that the local forcing amplitude results in the change of the rotating frequency of spiral wave. Our conclusions and discussion are given in Section 4.

2. Model

All simulations in the paper are based on a FitzHugh–Nagumo–type (FHN) model

$$\frac{\partial u}{\partial t} = f(u,v) + \nabla^2 u + G, \quad \frac{\partial v}{\partial t} = g(u,v). \tag{1}$$

The reaction kinetic functions $f(u,v)$ and $g(u,v)$ take the following forms:

$$f(u,v) = (u - u^3/3 - v)/\varepsilon, \tag{2}$$

$$g(u,v) = \varepsilon(u + \beta - \gamma v), \tag{3}$$

where u is the fast activator and v is the slow inhibitor, ε is a parameter characterizing the excitability of the medium. Parameters of $\varepsilon = 0.3$, $\beta = 0.61$, and $\gamma = 0.5$ are fixed in the simulation. All numerical computations are performed by the explicit Euler method using a five-point finite-difference representation of the Laplacian on a 520×520 array with a grid spacing $\Delta x = \Delta y = 0.15385$ and a time step of $\Delta t = 0.004$. A no-flux boundary condition is applied.

In addition, the last item G of Eq. (1) denotes a local forcing and takes the form

$$G = \sum_{i,j} A_{ij} \cos(\omega_f t + \phi), \tag{4}$$

where A_{ij} is the forcing amplitude and ω_f is the frequency. The forcing is localized in the domain with a radius of r_0 around the spiral tip. The summation is performed over the circular region restricted by $r \le r_0$. Here, r is the radius of the circular domain $r = \sqrt{(x_i - x_0)^2 + (y_j - y_0)^2}$, with (x_0, y_0) the coordinate of the spiral tip, and i and j are the integer numbers that correspond to the discretized x and y variables as $x_i = i\Delta x$, $y_j = j\Delta y$, respectively. The spiral tip position is identified by maximizing the vector product $|\nabla u \times \nabla v|$.

3. Numerical results

Using the model mentioned above, a suitable initial condition may induce a rigidly rotating spiral wave, which has been illustrated in Fig. 1(a). The power spectrum of the time-intensity series of $u(t)$, obtained by the FFT method is shown in Fig. 1(b). The peak indicates the natural frequency $\omega_0 = 0.62318$ of the spiral wave without perturbation.

The frequency of local periodic forcing is important in modulating the trajectory of the spiral tip. In Fig. 2 the simulation shows that the trajectories of spiral tip undergoes a transition. To be specific, when the frequency of local forcing (ω_f) is close to the natural frequency (ω_0) of the spiral wave, the spiral drifts along a straight line (see the path of the spiral tip in Fig. 2(b)).[11] However, the frequency to induce a resonant drift has a slight deviation from ω_0. In our simulation we have found that the resonant frequency is $\omega_{bf} = 0.9768\omega_0$. When ω_f is less than ω_{bf}, the trajectory of spiral's tip is an epicycloids-like orbit with inward petals (see Fig. 2(a)), when ω_f is more than ω_{bf}, the trajectory of spirals tip is a hypocycloid-like orbit with outward petals (see Fig. 2(c)).

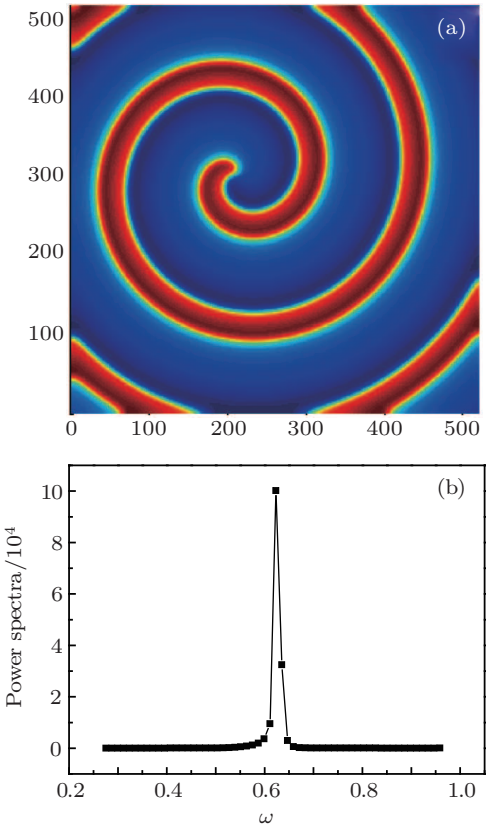


Fig. 1. (color online) (a) Snapshot of the fast activator u of a spiral wave without perturbation at $t = 360$ time units. (b) The power spectra from one site (20, 20) of system without control shows natural frequency $\omega_0 = 0.62318$. The parameters are: $\varepsilon = 0.3$, $D = 1.0$, $\beta = 0.61$, and $\gamma = 0.5$.

Second, we have found that it is important to select the appropriate radius of the local forcing control region for resonance drift. Different sizes to impose an LFP will result in different types of motion, even the amplitudes and frequencies of the LPF are the same. In Fig. 3, three types of spiral tip motion are displayed when changing the radius of the local forcing control region while the A and ω_f are kept. It can be found that the LFP with resonant frequency $\omega_f = 0.9768\omega_0$ at the case $r_0 = 10\Delta x$ leads to an inward motion at the case $r_0 = 7\Delta x$ and an outward motion at the case $r_0 = 13\Delta x$.

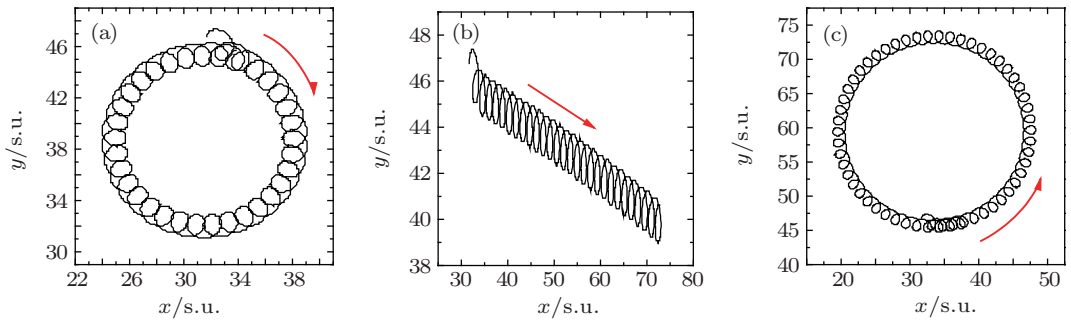


Fig. 2. (color online) The transition of trajectories of spiral tip by changing the frequency of a local periodic forcing. The amplitude of the local forcing is $A = 0.35$. Corresponding orbits are shown. (a) $\omega_{af} = 0.955\omega_0$, an epicycloids-like orbit with inward petals, (b) $\omega_{bf} = 0.9768\omega_0$, a straight line, (c) $\omega_{cf} = 0.992\omega_0$, a hypocycloid-like orbit with outward petals. We write the space and time units of the FitzHugh–Nagumo model as s.u. and t.u. respectively.

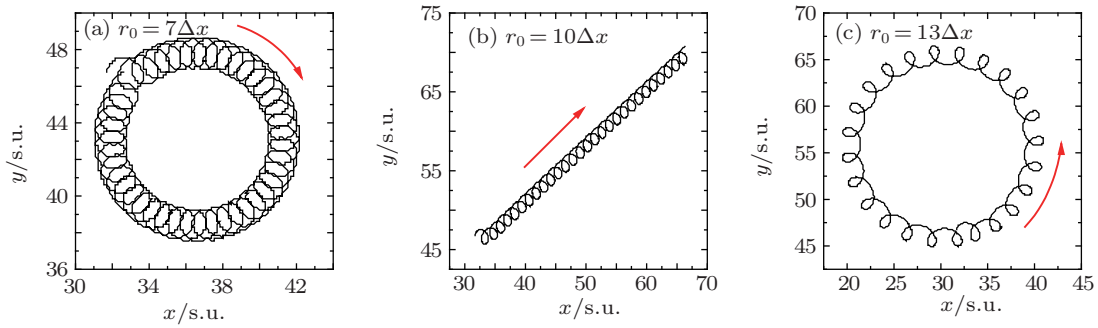


Fig. 3. (color online) The transition of trajectories of spiral tip induced by changing the radius (r_0) of local periodic forcing. The amplitude and frequency of local forcing are $A = 0.35$ and $\omega_f = 0.9768\omega_0$, respectively. The corresponding orbit is shown. (a) $r_0 = 7\Delta x$, an epicycloids-like orbit with inward petals; (b) $r_0 = 10\Delta x$, a straight line; (c) $r_0 = 13\Delta x$, a hypocycloid-like orbit with outward petals.

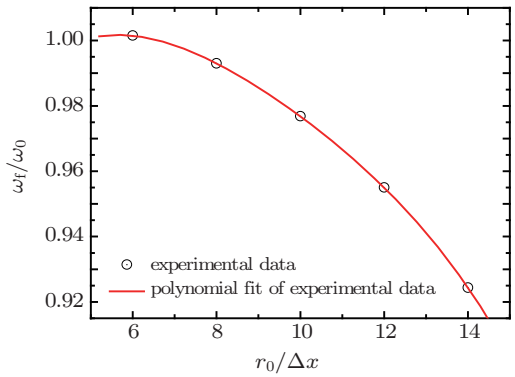


Fig. 4. (color online) Numerically determined FHN model resonant drift frequency ω_f as a function of the radius (r_0) of local forcing control region (the values in Table 1). The solid curve is drawn by the four-order polynomial fitting the simulation data (open circles).

Thus, if the radius of the control region to apply LFP is varied, the resonant frequency is changed correspondingly. In Table 1, we present the radii of local forcing control region and the corresponding resonance frequencies. In Fig. 4 we show the radius (r_0) of local forcing control region and the corresponding resonance drift frequencies ω_f. An obvious result is that the values of ω_f/ω_0 decrease with the increase of r_0. It is found that the numerical result ω_f from simulation can be fitted by the following function:

$$\omega_f(z) = (-0.0013802z^4 - 0.00036234z^3 - 0.0064479z^2 - 0.029897z + 0.9768)\omega_0. \quad (5)$$

Here, $z = (r - 10)/3.1623$.

Table 1. The radii of local forcing control region and the corresponding resonance frequencies.

$r_0/\Delta x$	6	8	10	12	14
ω_f/ω_0	1.0015	0.993	0.9768	0.955	0.9244

Third, we will investigate how the amplitude of the local forcing influences the natural frequency of the spiral wave. Here, the radius ($r_0 = 10\Delta x$) of the control region is fixed. Numerical simulations show that the resonant drift frequency slightly decreases with the increase of the amplitude of the local forcing; that is, the natural rotating frequency decreases accordingly. In Table 2, we present the amplitudes of local forcing and the corresponding resonance frequencies. In Fig. 5, we show the amplitude (A) of local forcing and the corresponding resonance drift frequency ω_f. It is found that the numerical result ω_f from our simulation can be fitted by the following function:

$$\omega_f(z) = (0.00022388z^4 + 0.00115z^3 - 0.0041963z^2 - 0.028833z + 0.97108)\omega_0. \quad (6)$$

Here, $z = (A - 0.38333)/0.15811$.

Table 2. The amplitudes of local forcing and the corresponding resonance frequencies.

A	0.15	0.2	0.25	0.3	0.35	0.4	0.45	0.5	0.55	0.6
ω_f/ω_0	100018	0.9976	0.9918	0.98495	0.9768	0.968	0.9585	0.948	0.9375	0.9275

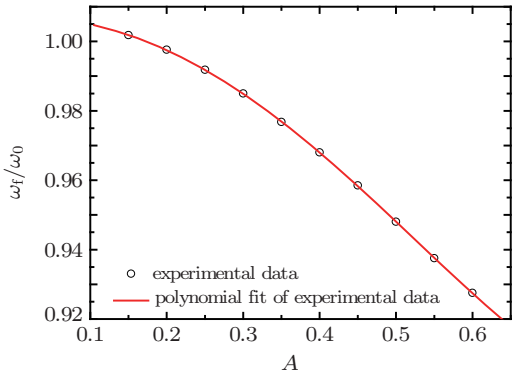


Fig. 5. (color online) Numerically determined FHN model resonant drift frequency ω_f as a function of the amplitudes (A) of local forcing (the values in Table 2). The solid curve is drawn by the four-order polynomial fitting the simulation data (open circles).

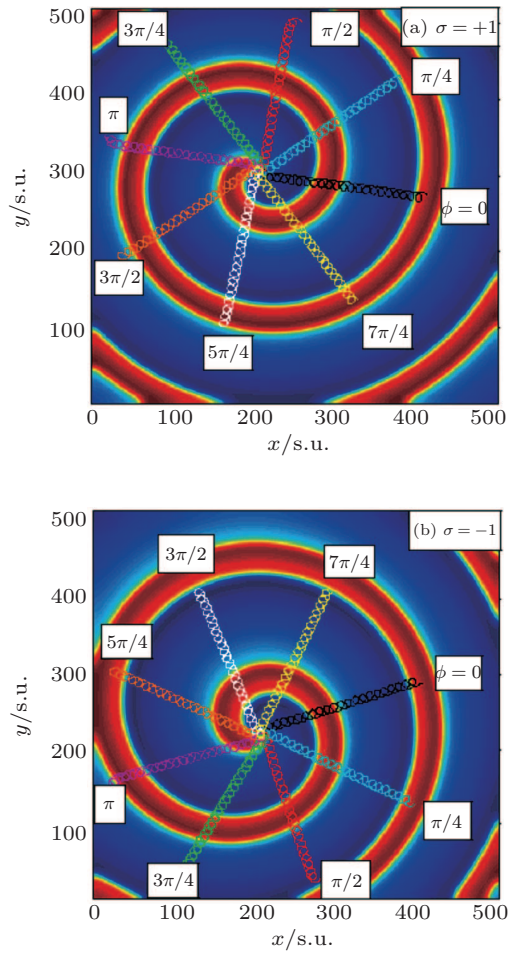


Fig. 6. (color online) Dependence of the drift by local periodic forcing with amplitude $A = 0.35$ on the phase shift (ϕ) at resonant frequency $\omega = \omega_{bf}$. (a) Tip path of anticlockwise ($\sigma = +1$) spiral; (b) tip path of clockwise ($\sigma = -1$) spiral. Parameters in the simulations are $\varepsilon = 0.3$, $\beta = 0.61$, $\gamma = 0.5$. The system size is 80×80, 520×520 grid points and $\Delta t = 0.004$ are used in our simulations. The no-flux boundary conditions are imposed.

Finally, we investigate the control of the resonant drift of a spiral under a LPF with frequency equal to that of the spiral. In Fig. 6, we present the drift paths of the spiral tip with different phase shifts at the resonant frequency $\omega_f = \omega_{bf}$. Figure 6(a) shows the tip's paths of an anticlockwise rotating spiral ($\sigma = +1$, $\sigma = \pm 1$ is the chirality of the spiral, $\sigma = +1$ for the anticlockwise rotating spiral, while it is $\sigma = -1$ for the clockwise one). It is clear that the direction of the drift can be efficiently controlled by changing the phase shift ϕ of the local forcing. For example, based on the potential application, we can select the optimal phase shift to force a spiral to drift out of the heart's surface in the shortest time. In addition, as shown in Fig. 6(a), the drift direction of the spiral tip will change linearly anticlockwise (for $\sigma = +1$) when increasing the phase shift ϕ. The plotted drift angles θ in Fig. 7(a) show a linear increase with ϕ for $\sigma = +1$.

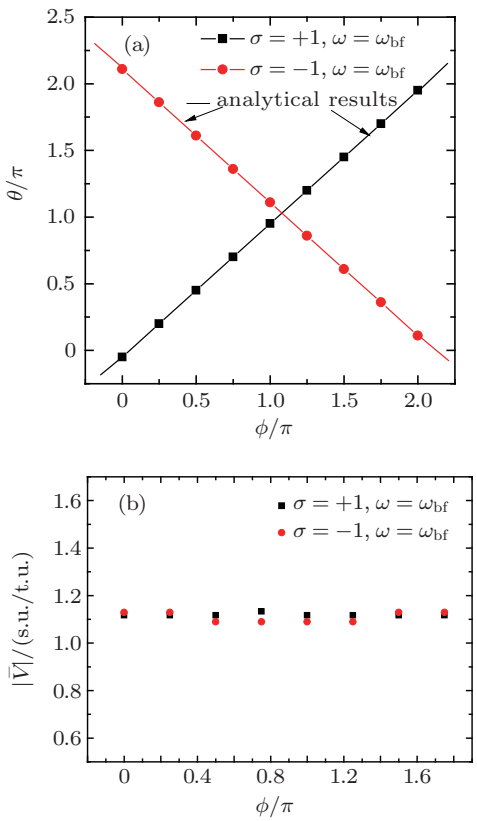


Fig. 7. (color online) The quantities θ (a) and $|\bar{V}|$ (b) plotted from drift trajectories vs ϕ for the resonant drift of spiral induced by the local forcing at $\omega = \omega_{bf}$. Parameters are selected as $A = 0.35$, $\varepsilon = 0.3$, $\beta = 0.61$, and $\gamma = 0.5$.

Furthermore, the chirality of a spiral affects its drift behavior. Compared with Fig. 6(a) ($\sigma = +1$), the drift direction changes clockwise when increasing the phase shift ϕ in

Fig. 6(b) ($\sigma=-1$). Accordingly, the drift angles θ in Fig. 7(a) decrease linearly as ϕ is increased for $\sigma=-1$.

While keeping the same amplitude of local forcing, we find that the velocities of drift in the same duration are almost identical (in Figs. 6(a) and 6(b)). In Fig. 7(b), the plotted average drift velocities are almost identical. This means that the drift velocity is independent of the chirality of the spiral.

In order to attain insight into the underlying mechanism of the resonant drift phenomenon, we make theoretical analysis by the weak deformation approximation method.[20]

Considering the influence of two arbitrary external fields $G_1(x,y,t)$ and $G_2(x,y,t)$ on the system (1), we obtain

$$\frac{\partial u}{\partial t}=f(u,v)+\nabla^2 u+G_1,\quad \frac{\partial v}{\partial t}=g(u,v)+G_2. \tag{7}$$

Supposing G_1 and G_2 induce a drift of the spiral tip with velocity $\boldsymbol{V}=[V_x(t),V_y(t)]$, then we can rewrite a parturbed equation in the moving frame of $\boldsymbol{V}$ as follows:

$$\begin{aligned}\frac{\partial u}{\partial t}&=f(u,v)+\nabla'^2 u+\boldsymbol{V}\cdot\nabla' u+G_1,\\ \frac{\partial v}{\partial t}&=g(u,v)+\boldsymbol{V}\cdot\nabla' v+G_2.\end{aligned} \tag{8}$$

Considering G_1 and G_2 are small and located near the spiral tip, the deformation of the spiral around the tip is weak, all the values of u, v and their derivatives around the tip in the moving frame are unchanged compared with those of the unperturbed spiral around the tip.[20]

Based on this approximation, we can obtain the drift velocity of the spiral tip as follows:

$$\begin{aligned}V_x(t)&=[(-G_1v_y+G_2u_y)/(u_xv_y-u_yv_x)]_{\rm tip},\\ V_y(t)&=[(G_1v_x-G_2u_x)/(u_xv_y-u_yv_x)]_{\rm tip},\end{aligned} \tag{9}$$

where $u_x=a_1\cos(\omega_0t-\alpha)$, $u_y=\sigma a_1\sin(\omega_0t-\alpha)$, $v_x=a_2\cos(\omega_0t-\delta)$, $v_y=\sigma a_2\sin(\omega_0t-\delta)$, and $u_xv_y-u_yv_x=\sigma a_1a_2\sin(\alpha-\delta)$. Here, a_1 and a_2 are coefficients, α and δ are two phase shifts, $\sigma=\pm1$ is the chirality of the spiral, ω_0 is the rotating frequency.

Comparing Eq. (1) with Eq. (7), one can see $G_1=\sum_{i,j}A_{ij}\cos(\omega_{\rm f}t+\phi)$ and $G_2=0$. Then, we obtain an approximate formula

$$\begin{aligned}V_x(t)&=\frac{c}{2}[\sin((\omega_{\rm f}+\omega_0)t+\phi-\delta)\\ &\quad+\sin((\omega_{\rm f}-\omega_0)t+\phi+\delta)],\\ V_y(t)&=-\sigma\frac{c}{2}[\cos((\omega_{\rm f}+\omega_0)t+\phi-\delta)\\ &\quad+\cos((\omega_{\rm f}-\omega_0)t+\phi+\delta)],\end{aligned} \tag{10}$$

where $c=A_{ij}/[a\sin(\delta-\alpha)]$, By substituting $\omega_{\rm f}=\omega_0$ in Eq. (10), equation (10) can be simplified as

$$V_x(t)=\frac{c}{2}\left[\sin(2\omega_0t+\phi-\delta)+\sin(\phi+\delta)\right],$$

$$V_y(t)=-\sigma\frac{c}{2}\left[\cos(2\omega_0t+\phi-\delta)+\cos(\phi+\delta)\right]. \tag{11}$$

Therefore, the formula of drift velocity of the spiral tip is obtained, and the resonant drift behavior in the simulation is confirmed by our theoretical analysis. By integrating Eq. (11) on time t, a simple expression of the drift velocity is obtained

$$\begin{aligned}\bar{V}_x(t)&=\frac{c}{2T}\int_0^T[\sin(2\omega_0t+\phi-\delta)+\sin(\phi+\delta)]\,{\rm d}t\\ &=\frac{c}{2}\sin(\phi+\delta),\\ \bar{V}_y(t)&=-\sigma\frac{c}{2T}\int_0^T[\cos(2\omega_0t+\phi-\delta)+\cos(\phi+\delta)]\,{\rm d}t\\ &=-\sigma\frac{c}{2}\cos(\phi+\delta),\end{aligned} \tag{12}$$

where $T=2\pi/\omega_0$. Thus, the constant drift velocity amplitude $|\boldsymbol{V}|$ and the drift angle θ are obtained as follows:

$$|\boldsymbol{V}|=\sqrt{\bar{V}_x^2+\bar{V}_y^2}=\frac{|c|}{2}=\left|\frac{A_{ij}}{2a_1\sin(\delta-\alpha)}\right|, \tag{13}$$

$$\tan\theta=\frac{\bar{V}_y}{\bar{V}_x}=\sigma\tan(\phi+\delta+\pi/2), \tag{14}$$

$$\theta=\sigma(\phi+\delta+\pi/2)+k\pi. \tag{15}$$

From Eq. (13), one can see that the drift velocity is proportional to the amplitude A_{ij} of the local forcing. However, it has nothing to do with the phase shift $\phi$and chirality σ, which is consistent with the simulation results in Figs. 6 and 7(b). From Eq. (15), one can also see that the drift angle θ of the spiral tip will increase clockwise when the phase ϕ is increased for $\sigma=+1$, while the drift angle θ of the spiral tip will increase anticlockwise when the phase ϕ is increased for $\sigma=-1$. These results are confirmed by our numerical simulations in Fig. 7(a).

4. Conclusion and discussion

In conclusion, we have studied a method to control the motion of a spiral wave using a local periodic forcing around the spiral tip. Three types of spiral tip motion are observed: the epicycloids-like meandering with inward petals, the resonant drift, and the hypocycloid-like meandering with outward petals. First, the size of region where LPF is imposed will change the resonant frequency. The bigger the size, the smaller the value of $\omega_{\rm f}/\omega_0$ will be. Second, the strength of the local forcing will also change the resonant frequency. The stronger the forcing, the smaller the value of $\omega_{\rm f}/\omega_0$ will be. These quantitative relations are presented. We, therefore, conclude that the size of region where LPF is imposed and the strength of local forcing should play an important role for the spiral wave control. It is shown that the velocity and direction of resonant drift can be efficiently controlled by changing

the amplitude and phase shift of the local periodic forcing, respectively. Our theoretical analytical results based on weak deformation approximation are consistent perfectly with the simulation results.

Finally, we have to emphasize that the model used in this paper is very simple for simulating actual cardiac models. A real heart is a nonuniform complex system. Therefore, further study taking into account more realistic cardiac activities is needed in the future. We hope that our results will help to improve the control scheme and so reduce tissue damage. Nevertheless, some crucial problems for the applications to cardiac tissue are still not solved.

References

[1] Meron E 1992 *Phys. Rep.* **218** 1
[2] Lechleiter J, Girard S, Peralta E and Clapham D 1991 *Science* **252** 123
[3] Davidenko J, Pertsov A, Salomonsz R, Baxter W and Jalife J 1992 *Nature* **355** 349
[4] Plapp B B, Egolf D A, Bodenschatz E and Pesch W 1998 *Phys. Rev. Lett.* **81** 5334
[5] Winfree T 1991 *Chaos* **1** 303
[6] Steinbock O, Zykov V and Müller S C 1993 *Nature* **366** 322
[7] Ouyang Q and Flesselles J M 1996 *Nature* **379** 143
[8] Jahuke W and Winfree A T 1991 *Int. J. Bifurc. Chaos* **1** 445
[9] Zykov V S, Steinbock O and Müller S C 1994 *Chaos* **4** 509
[10] Guo H, Liao H M and Ouyang Q 2002 *Phys. Rev. E* **66** 026104
[11] Zhan M, Wang X G, Gong X F and Lai C H 2005 *Phys. Rev. E* **71** 036212
[12] Mantel R M and Barkley D 1996 *Phys. Rev. E* **54** 4791
[13] Zhang H, Cao Z J, Wu N J, Ying H P and Hu G 2005 *Phys. Rev. Lett.* **94** 188301
[14] Yuan G Y, Wang G R and Chen S G 2005 *Europhys. Lett.* **72** 908
[15] Wu N J, Zhang H, Ying H P, Cao Z J and Hu G 2006 *Phys. Rev. E* **73** 060901
[16] Zykov S, Zykov V and Davydov V 2006 *Europhys. Lett.* **73** 335
[17] Yu L C, Ma J, Zhang G Y and Chen Y 2008 *Chin. Phys. Lett.* **25** 2706
[18] Zykov V S, Bordiougov G, Brandtstädter H, Gerdes I and Engel H 2004 *Phys. Rev. Lett.* **92** 018304
[19] Zhang H, Wu N J, Ying H P, Hu G and Hu B B 2004 *J. Chem. Phys.* **121** 7276
[20] Liu G Q, Wu N J and Ying H P 2013 *Commun. Nonlinear Sci. Numer. Simulat.* **18** 2398
[21] Steinbock O, Schütze J and Müller S C 1992 *Phys. Rev. Lett.* **68** 248
[22] Munuzuri A P, Gesteira M G and Munuzuri V P 1994 *Phys. Rev. E* **50** 4258
[23] Chen J X and Hu B B 2008 *Europhysics. Lett.* **84** 34002
[24] Lou Q, Chen J X, Zhao Y H, Shen F R, Fu Y, Wang L L and Liu Y 2012 *Phys. Rev. E* **85** 026213
[25] Grill S, Zykov V S and Müller S C 1995 *Phys. Rev. Lett.* **75** 3368
[26] Zykov V S, Mikhailov A S and Müller S C 1990 *Phys. Rev. Lett.* **78** 3398
[27] Ott E, Grebogi C and Yorke J A 1990 *Phys. Rev. Lett.* **64** 1196
[28] Yuan G Y, Xu A G, Wang G R and Chen S G 2010 *Europhys. Lett.* **90** 10013
[29] Zhang G Y, Ma J, Yu L C and Chen Y 2008 *Chin. Phys. B* **17** 4107
[30] Yuan G Y, Yang S P, Wang G R and Chen S G 2005 *Acta Phys. Sin.* **54** 1510 (in Chinese)
[31] Zhang H J, Wang P Y and Zhao Y Y 2005 *Chin. Phys. Lett.* **22** 287
[32] Deng B W, Zhang G Y and Chen Y 2008 *Commun. Theor. Phys.* **52** 173
[33] Ma J, Wang C N, Jin W Y, Li Y L and Pu Z S 2008 *Chin. Phys. B* **17** 2844
[34] Wu N J, Gao H J and Ying H P 2010 *Phys. Rev. E* **82** 066206
[35] Markus M, Magy-Ungvaray Z and Hess B 1992 *Science* **257** 225
[36] Xu L D, Qu Z L and Di Z R 2009 *Phys. Rev. E* **79** 036212
[37] Xu L D, Li Z, Qu Z L and Di Z R 2012 *Phys. Rev. E* **85** 046216
[38] Chen J X, Xu J R, Zhang X P, Zhang J W and Zhang X W 2009 *Cent. Eur. J. Phys.* **7** 108
[39] Cao Z J, Li P F, Zhang H and Hu G 2007 *Chaos* **17** 0151071
[40] Chen J X, Mao J W, He Y F, Hu B B, Xu J R and Yuan X P 2009 *Phys. Rev. E* **79** 066209
[41] Zykov S, Zykov V S and Davydov V 2006 *Europhys. Lett.* **73** 335
[42] Wu N J, Li B W and Ying H P 2006 *Chin. Phys. Lett.* **23** 2030